Interface deformations due to counter-rotating vortices: Viscous versus elastic media

Jacco H. Snoeijer[1,2] and Leen van Wijngaarden[1]

[1]*Physics of Fluids Group and J. M. Burgers Centre for Fluid Dynamics, University of Twente, P.O. Box 217, 7500 AE Enschede, The Netherlands*

[2]*Mesoscopic Transport Phenomena, Eindhoven University of Technology, Den Dolech 2, 5612 AZ Eindhoven, The Netherlands*

(Received 6 December 2014; published 2 March 2015)

Capillary forces determine the shape of a liquid interface. Although often not considered, elastic solids with a free surface are also subjected to surface forces and these become important for materials of low Young's modulus. Here we consider two equivalent problems where a capillary free surface deforms due to vortices: (i) in a steady viscous flow [solved by Jeong and Moffatt, J. Fluid Mech. **241**, 1 (1992)], and (ii) in an elastic medium. The equations of linear incompressible elasticity and viscous flow are strictly identical, and the two-dimensional problems that we consider are solved using complex variable methods. Despite the similarity, the kinematics of the free surface is very different for the viscous and elastic cases. We show for the present problem that these kinematics result in displacement and velocity fields of different topology. Unexpectedly, the resulting surface deflections are even of opposite sign.

DOI: 10.1103/PhysRevE.91.033001 PACS number(s): 47.55.nb, 68.03.Cd, 46.25.−y

I. INTRODUCTION

Liquid menisci are shaped by capillary forces, following the classical laws established by Young and Laplace [1]. Recently, there is growing interest in how interfacial forces can determine the shape of very soft *solids*, such as gels and elastomers. For example, it was found that a cylinder of agar gel of low elastic modulus undergoes a Rayleigh-plateau-like instability [2]. Just like liquids, soft elastic media are thus susceptible to a Laplace pressure due to surface stress whenever their interface is curved [3]. Similar conclusions were drawn for the rounding of sharp edges [4,5] and indentation of soft layers by liquid drops [6–12] or by rigid bodies [13,14], as well as for the propagation of surface waves [15,16]. In all cases, the ratio of surface tension γ and shear modulus μ defines a length scale over which capillary effects are important. For glass or steel this length scale γ/μ is smaller than the molecular size, while for gels it can be as large as 10 to 100 μm. In the latter case, elastocapillary deformations are thus significant and within the range of microscopy techniques [17–19].

The analogy between liquid and elastic media carries over to other properties as well. Like liquids, very soft gels usually have a Poisson ratio $\nu \approx 0.5$ and are thus essentially incompressible. This is due to the fact that such materials are typically composed of a cross-linked network of incompressible polymer melt, or a network that contains an incompressible solvent. In addition, the equations for highly viscous flows are mathematically *identical* to those of linear elasticity for incompressible media. Namely, creeping flows are governed by the Stokes equation complemented with incompressibility:

$$\nabla p = \eta \nabla^2 \mathbf{v}, \quad \nabla \cdot \mathbf{v} = 0, \tag{1}$$

where η is the viscosity, $\mathbf{v}$ the velocity field, and p the pressure field. Exactly the same set of equations describes the displacement field $\mathbf{u}$ in an incompressible elastic medium, the Navier equations, which at steady state give

$$\nabla p = \mu \nabla^2 \mathbf{u}, \quad \nabla \cdot \mathbf{u} = 0. \tag{2}$$

Again, μ is the shear modulus of the solid. Indeed, this mathematical equivalence was exploited on numerous occasions, where viscous flow problems were solved using methods borrowed from linear elasticity. A well-known example is the use of the Michell solution [20], used, e.g., for two-dimensional corner flow problems [21–26]. Other notable examples are free surface cusps [27] and the coalescence of viscous drops [28,29], which are analyzed using complex variable methods developed for linear elasticity [30].

In this paper we investigate the viscous flow–linear elasticity analogy for the two-dimensional problem of free surface deformation induced by counter-rotating vortices [31]. The flow induced inside a viscous liquid was determined analytically by Jeong and Moffatt [27], by considering a vortex dipole placed at a distance d below the free surface. This situation is sketched in Fig. 1(a). Using complex variable methods, it was demonstrated that the free surface develops a sharp, steady cusp at large dipole strength. Later studies have focused on the entrainment of air through such a cusp [32,33]. The flow field appearing at small strength, i.e., for vanishing interface deflection, is shown in Fig. 1(b). The downward flow along the center line is responsible for pulling down the interface. The goal of the present paper is to solve the problem of the elastic equivalent, where a *displacement vortex dipole* (generated by a torque dipole) is placed inside an elastic body with a free surface. A physical realization of this problem can be achieved by embedding two rigid cylinders inside an elastic gel—exerting an opposite torque on both cylinders will create a displacement field that can be idealized by a vortex dipole. Despite the analogy with viscous flow, we demonstrate that the resulting displacement fields [Fig. 1(c)] are fundamentally different from the viscous flow fields [Fig. 1(b)]. In the elastic case the interface is actually pushed upwards, farther away from the dipole singularity. We demonstrate how this originates from differences in the kinematics of the free surface.

In Sec. II we analyze the problem by dimensional analysis and present the complex variable formalism. The elastic problem is solved by conformal mapping to the unit circle in Sec. III, with and without the presence of surface tension forces at the interface. We conclude in Sec. IV.

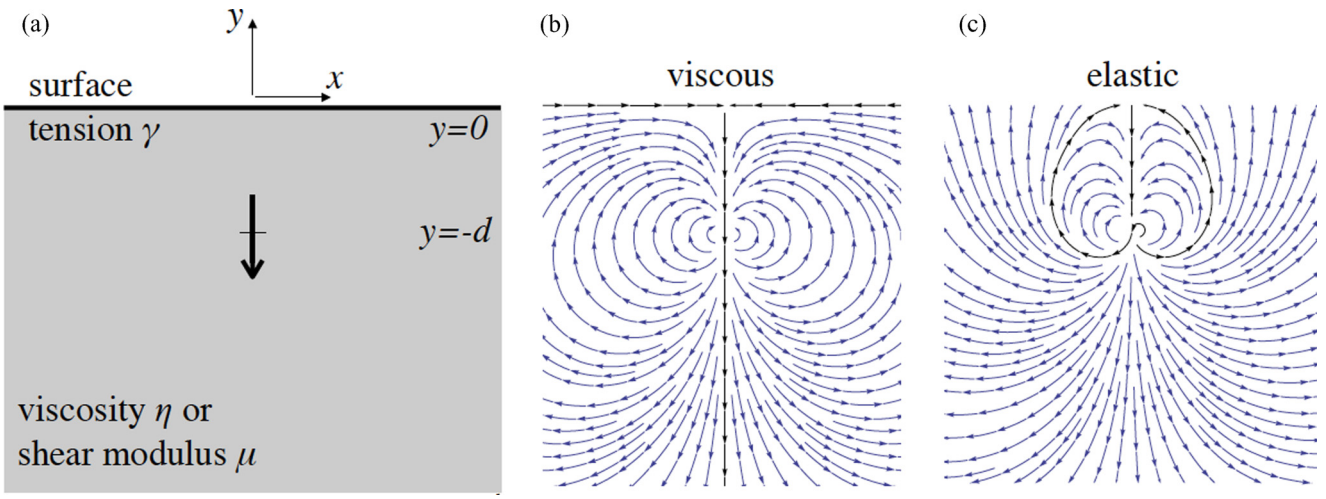

FIG. 1. (Color online) (a) Problem sketch: A vortex dipole is placed at a distance d below an interface of surface tension γ. We compare the resulting interface deflection for the cases where the medium is viscous (with viscosity η) or elastic (incompressible, with shear modulus μ). (b) Velocity field in a steady viscous flow at very small dipole strength, as computed by Jeong and Moffatt [27]. The flow is such that the free surface is drawn downwards, although the deflection in this case has a vanishing amplitude [i.e., small capillary number in Eq. (3)]. The boundary condition for steady flow is that the free surface is a streamline. (c) Elastic displacement field in an incompressible elastic medium, here taken with vanishing surface tension. The free surface is no longer a streamline: All streamlines outside the dark contour cross the free surface and deflect the interface upwards.

II. FORMULATION

A. Steady viscous flow versus elasticity

1. Dimensional analysis

Let us first recall the essentials of the viscous problem of interest. A vortex dipole of strength α (dimension m^3/s) is imposed in a viscous medium of viscosity η, at a distance d below an interface of surface tension γ. We consider solutions for which the interface is deformed, but steady. The problem is characterized by a single dimensionless parameter, the capillary number $\mathcal{C} = \eta\alpha/\gamma d^2$. This parameter quantifies the driving strength and determines the amount of free surface deflection. At small driving the surface deflection $h(x)$ can be obtained from a perturbation analysis, which for $\mathcal{C} \ll 1$ reads [27]

$$\frac{h(x)}{d} = -\frac{4\mathcal{C}}{(x/d)^2+1}. \tag{3}$$

The minus sign in front of the expression shows that the interface is drawn downwards by the vortex dipole. Interestingly, the free surface develops a cusp in the limit of large $\mathcal{C}$, with a diverging curvature [27,33]. Apart from the very small radius of curvature of the tip of the cusp, the scale of the global deflection is still determined by d.

The equivalent elastic problem is achieved by imposing a dipole vortex of the *displacement* field (rather than of the velocity field) in an incompressible elastic medium of shear modulus μ. The strength of this vortex dipole is β (dimension m^3), which can be made dimensionless by the distance d at which it is placed below the free surface. Hence, a first dimensionless parameter is

$$\mathcal{B} = \frac{\beta}{d^3}. \tag{4}$$

As this dimensional argument already suggests, it turns out that the elastic problem is well defined even without the introduction of surface tension. This is to be contrasted with the viscous case: To achieve a steady state, one requires surface tension (or another field such as gravity) in order to balance the time scale from α. Still, the elastic free surface does possess a surface tension γ, so that a second dimensionless number appears:

$$\Gamma = \frac{\gamma}{\mu d}. \tag{5}$$

This parameter can be seen as a ratio of length scales, where γ/μ is the elastocapillary length previously referred to. In linear response to the vortex dipole, we anticipate that the surface deflection will be of the form

$$\frac{h(x)}{d} = \mathcal{B} f(x/d,\Gamma). \tag{6}$$

The central goal of the paper will be to compute the elastic displacement field inside the elastic medium, and the resulting surface shape characterized by $f(x/d,\Gamma)$.

2. Boundary conditions

Since the equations of viscous flow and linear elasticity are strictly identical, the differences above must find their origin in the boundary conditions. The conditions of normal and tangential stress at the free surface are identical, i.e.,

$$\sigma_{nn} = \gamma\kappa, \quad \sigma_{nt} = 0, \tag{7}$$

where κ is the interface curvature

$$\kappa = \frac{h''}{(1+h'^2)^{3/2}}. \tag{8}$$

To be precise, the factor γ in (7) is the surface stress. For the elastic interface surface this can be different from its surface free energy, due to the thermodynamic relation by Shuttleworth [34–36]. Here we simply refer to this material property as the surface tension.

The key difference occurs for the *kinematic* boundary condition that relates the viscous and elastic fields to the free

surface shape $h(x)$. To achieve steady state in the case of flow, the velocity field needs to be parallel to the free surface. In terms of the field components v_x, v_y this implies

$$\frac{dh}{dx} = \left(\frac{v_y}{v_x}\right)_{x,y=h(x)}. \tag{9}$$

By contrast, the elastic free surface is defined by

$$h(x) = u_y|_{x,y=0}, \tag{10}$$

which needs to be evaluated at the boundary of the undeformed body (i.e., at $y = 0$). These different kinematic conditions greatly affect the respective fields. For instance, a steady fluid interface must be the streamline of the field, which is manifestly not the case for an elastic boundary [cf. Figs. 1(b) and 1(c)].

The kinematic conditions (9) and (10) are also very different from a dimensional point of view. The viscous case (9) involves a *ratio* of velocity components, so that knowledge of the velocity scale $\sim\alpha/d^2$ is not sufficient to know the typical magnitude of the deflection dh/dx. The stress balance between surface tension and viscosity is explicitly needed to determine the ratio. By contrast, for the elastic case without surface tension one immediately has $h \sim u_y \sim \beta/d^2$. Addition of surface tension will of course influence the final shape of the interface.

B. Complex variable formulation of linear elasticity

The two-dimensional elastic problem is solved by complex variable methods, following the classical approach in [30]. We briefly summarize the key relations that are needed for our analysis. The formulation is based on the Airy stress function $\mathcal{U}(x,y)$, which satisfies the biharmonic equation $\nabla^4\mathcal{U} = 0$. Introducing the complex variable $z = x + iy$, the general solution can be written as

$$\mathcal{U} = \mathrm{Re}\left[\overline{z}\phi(z) + \chi(z)\right], \tag{11}$$

where the functions $\phi(z)$ are $\chi(z)$ are holomorphic on the elastic domain. The overbar means the complex conjugate. Introducing the complex displacement $u = u_x + iu_y$, one finds for an incompressible elastic body

$$2\mu u = \phi(z) - z\overline{\phi'(z)} - \overline{\psi(z)}, \tag{12}$$

where $\psi(z) = \chi'(z)$. Similarly to the displacement, the stress components can be expressed in terms of the "potentials" $\phi(z)$ and $\psi(z)$. For the purpose of the present paper, the key equation comes from the stress boundary condition. Defining $T_x + iT_y$ as the traction vector at the boundary, one can express the boundary condition as the integral [30]

$$\phi(z) + z\overline{\phi'(z)} + \overline{\psi(z)} = i\int ds(T_x + iT_y). \tag{13}$$

This equation applies for z along the boundary contour, while s is the curvilinear coordinate along the contour.

For the geometry shown in Fig. 1(a), the contour is defined by $y = 0$ or $z = x$. The traction then relates to the stress components as $T_x + iT_y = \sigma_{xy} + i\sigma_{yy}$. The integration can be performed using $ds = -dx$, where the minus sign ensures the convention that the integral requires the elastic domain to be on the left. The condition that the interface has no shear stress, i.e., $T_x = 0$, allows for an important simplification. In that case the left-hand side of (13), which we recall to be valid along the free surface, has no imaginary part. Combined with (12), this gives the displacement at the free surface,

$$h(x) = u_y(x,0) = \frac{1}{\mu}\{\mathrm{Im}\left[\phi(z = x)\right] + K\}. \tag{14}$$

Here we introduced a constant K, since adding a constant to the potentials does not change the stress or strain field, but gives a rigid body translation. Below the constant K will be chosen such that $h(\pm\infty) = 0$.

Finally we point out the connection to the viscous flow formulation, which is commonly based on the stream function $\Psi(x,y)$. The stream function also satisfies the biharmonic equation $\nabla^4\Psi = 0$, such that a similar complex variable method can be applied. By definition of the stream function one has

$$u_x + iu_y = \frac{\partial\Psi}{\partial y} - i\frac{\partial\Psi}{\partial x}, \tag{15}$$

where for the present purpose we readily consider the field $u_x + iu_y$ to be the displacement vector. Compared to the formulation (12), one then obtains

$$\Psi = -\frac{1}{2\mu}\mathrm{Im}\left[\overline{z}\phi(z) + \chi(z)\right], \tag{16}$$

which indeed satisfies $\nabla^4\Psi = 0$. This expression is convenient in order to draw the "streamlines" of the displacement field, which are defined by contours of constant $\Psi(x,y)$. Note that the introduction of the stream function in the elastic problem applies only when the medium is incompressible.

The vortex dipole will be introduced in the same manner as suggested by Jeong and Moffatt [27], who imposed it as a singularity in the stream function. In the present notation this becomes

$$\psi \simeq \frac{2i\mu\beta}{(z + id)^2}, \tag{17}$$

giving the dipole singularity at $z = -id$, while $\phi(z)$ is holomorphic on the entire domain. This singularity in ψ can be seen as a *torque* dipole per unit length, of strength $2\mu\beta$ (dimension N m). This represents the stress field necessary to generate the vortex dipole of strength β.

III. SOLUTION FOR THE ELASTIC FREE SURFACE

From now on we will use dimensionless variables. Distances are scaled with d, while as anticipated $\mathcal{B} = \beta/d^3$ and $\Gamma = \gamma/\mu d$. Stresses are scaled with μ, and the potentials ϕ and ψ are made dimensionless with μd. We will first consider the case without surface tension to illustrate the solution method ($\Gamma = 0$, Sec. III A), before turning to the influence of capillarity ($\Gamma \neq 0$, Sec. III B). The resulting displacement fields will be illustrated and discussed in Sec. III C.

A. Neglecting surface tension

To illustrate the solution scheme, we first consider the problem without surface tension, so that both boundary stresses $\sigma_{xy} = \sigma_{yy} = 0$ at the free surface. Within linear elasticity theory, the fields are defined on the undeformed domain and as a consequence the boundary conditions are

imposed at $z = x$ (i.e., $y = 0$). In terms of the complex potentials, the boundary condition at the free surface reads

$$\phi(z) + z\overline{\phi'(z)} + \overline{\psi(z)} = 0, \tag{18}$$

valid at $z = x$. The boundary condition is homogeneous, but we obtain a nontrivial solution when imposing the torque-dipole singularity at $z = -i$ as

$$\psi(z) \simeq \frac{2\mathcal{B}i}{(z+i)^2}. \tag{19}$$

This is the dimensionless form of (17), with again $\mathcal{B} = \beta/d^3$. The singularity will serve as a "forcing" of the solution.

To solve for the potentials, we will use the conformal map

$$z = w(\zeta) = i\frac{\zeta - i}{\zeta + i}, \tag{20}$$

which maps the undeformed surface $z = x$ to the unit circle $|\zeta| = 1$. The center of the circle ($\zeta = 0$) corresponds to the position of the dipole singularity ($z = -i$). We introduce auxiliary potentials $F(\zeta)$ and $G(\zeta)$, defined as

$$F(\zeta) = \phi(w(\zeta)) = \phi(z), \tag{21}$$

$$G(\zeta) = \psi(w(\zeta)) = \psi(z). \tag{22}$$

Hence, $\phi'(z) = F'(\zeta)/w'(\zeta)$. Working out the derivative w', we obtain

$$z\overline{\phi'(z)} = \frac{w(\zeta)}{\overline{w'(\zeta)}}\overline{F'(\zeta)} = \frac{i}{2}\left(1 + \frac{1}{\zeta^2}\right)\overline{F'(\zeta)}, \tag{23}$$

where we used the fact that at the unit circle $\overline{\zeta} = 1/\zeta$. The boundary condition (18) then becomes

$$F(\zeta) + \frac{i}{2}\overline{[(1+\zeta^2)F'(\zeta)]} + \overline{G(\zeta)} = 0, \tag{24}$$

valid at the unit circle $|\zeta| = 1$.

The equation can be solved by assuming $F(\zeta)$ to be holomorphic inside the unit circle ($|\zeta| \leqslant 1$), while $G(\zeta)$ exhibits the dipole singularity. The singularity is split off by writing

$$G(\zeta) = \frac{iB}{\zeta^2} + H(\zeta), \tag{25}$$

and $H(\zeta)$ is again holomorphic for $|\zeta| \leqslant 1$. The correct strength of the singularity (19) is obtained by taking $B = \mathcal{B}/2$. With this, we can write (24) as

$$F(\zeta) + \frac{i}{2}\overline{[(1+\zeta^2)F'(\zeta)]} + \overline{H(\zeta)} = iB\zeta^2, \tag{26}$$

valid at $|\zeta| = 1$. This is an inhomogeneous linear equation for the holomorphic functions $F(\zeta)$ and $H(\zeta)$. Indeed, the singularity of the strength B provides the forcing for the elastic displacements.

Using the standard procedure described in [30], we can solve for the individual potentials by dividing (26) by $2\pi i(\sigma - \zeta)$ and integrating by $d\sigma$ along the the unit circle, i.e., $\sigma = e^{i\theta}$. For terms holomorphic inside and on the contour, like F, we can apply Cauchy's integral formula and the integration yields $F(\zeta)$ for all $|\zeta| \leqslant 1$. By contrast, the conjugate $\overline{F}$ of a holomorphic function gives a constant after integration, namely, $\overline{F(0)}$, which is a consequence of the contour being the unit circle [30]. Since constants represent a gauge invariance of the complex potentials, they can be omitted, so that this procedure effectively removes conjugates of holomorphic terms. This is the reason for mapping the boundary value problem from z to the unit circle in ζ. Hence, (26) yields after integration

$$F(\zeta) = iB\zeta^2, \tag{27}$$

valid for all $|\zeta| \leqslant 1$, i.e., on the entire elastic domain. The function $H(\zeta)$ can be obtained by applying the same procedure to the conjugate of (26). This gives

$$-\frac{i}{2}(1+\zeta^2)F'(\zeta) + H(\zeta) = 0, \tag{28}$$

again for all $|\zeta| \leqslant 1$. Hence, we obtain the auxiliary potentials

$$F(\zeta) = iB\zeta^2, \tag{29}$$

$$G(\zeta) = \frac{iB}{\zeta^2} - B\left(\zeta + \zeta^3\right). \tag{30}$$

The final step is now to invert the conformal map

$$\zeta = w^{-1}(z) = -i\left(\frac{z+i}{z-i}\right), \tag{31}$$

so that

$$\phi(z) = F(w^{-1}(z)) = -\frac{i\mathcal{B}}{2}\left(\frac{z+i}{z-i}\right)^2, \tag{32}$$

$$\psi(z) = G(w^{-1}(z)) = -\frac{i\mathcal{B}}{2}\left(\frac{z-i}{z+i}\right)^2 + \frac{i\mathcal{B}}{2}\left[\left(\frac{z+i}{z-i}\right) - \left(\frac{z+i}{z-i}\right)^3\right], \tag{33}$$

where we used $B = \mathcal{B}/2 = \beta/(2d^3)$. One verifies that these potentials indeed satisfy (18) for any real-valued $z = x$.

The displacement field corresponding to the solution (32) and (33) is sketched in Fig. 1(c). Our main interest is to find the surface deflection, which using (14) is given by the vertical displacement $h(x) = u_y(x, y = 0) = \mathrm{Im}[\phi(z = x)] + K$. This reads

$$\phi(x) = -\frac{i\mathcal{B}}{2}\frac{(x+i)^4}{(x^2+1)^2}, \tag{34}$$

which approaches $-i\mathcal{B}/2$ for $x \to \pm\infty$. Since we impose vanishing displacements at large distance, we need $K = \mathcal{B}/2$, and we obtain the surface deformation

$$h(x) = 4\mathcal{B}\frac{x^2}{(x^2+1)^2} = \frac{4\beta}{d^3}\frac{x^2}{(x^2+1)^2}. \tag{35}$$

B. Including surface tension

1. *Solution*

When the surface tension γ is included in the description, the normal stress boundary condition is given by the Laplace pressure jump. Since lengths and stresses are scaled with d

and μ respectively, this takes the dimensionless form

$$\sigma_{yy} = \Gamma \frac{\partial^2 u_y}{\partial x^2}, \tag{36}$$

with $\Gamma = \gamma/(\mu d)$ as before. Here we assumed a small deflection $(\partial u_y/\partial x)^2 \ll 1$. Due to this inhomogeneous boundary condition, the right-hand side of (13) becomes

$$i \int ds (T_x + i T_y) = -\Gamma \int ds \, \frac{\partial^2 u_y}{\partial x^2}. \tag{37}$$

Using $ds = -dx$ this is integrated to give

$$-\Gamma \int ds \, \frac{\partial^2 u_y}{\partial x^2} = \Gamma \frac{\partial u_y}{\partial x} = \frac{\Gamma}{2i}[\phi'(z) - \overline{\phi'(z)}], \tag{38}$$

where in the last step we once again used $u_y(x, y = 0) = \mathrm{Im}[\phi(z = x)] + K$. The boundary condition then becomes

$$\phi(z) + z\overline{\phi'(z)} + \overline{\psi(z)} = \frac{\Gamma}{2i}[\phi'(z) - \overline{\phi'(z)}], \tag{39}$$

valid at $z = x$.

As above, the problem is solved by mapping it onto the unit circle using $z = w(\zeta)$. In terms of the auxiliary potentials $F(\zeta) = \phi(z)$ and $G(\zeta) = \psi(z)$, the boundary condition (39) becomes

$$\begin{aligned} F(\zeta) + \frac{i}{2}[\overline{(1+\zeta^2)F'(\zeta)}] + \overline{G(\zeta)} \\ = -\frac{\Gamma}{4i}[(\zeta+i)^2 F'(\zeta) - \overline{(\zeta+i)^2 F'(\zeta)}]. \end{aligned} \tag{40}$$

Introducing once more the singularity using (25), this becomes

$$\begin{aligned} F(\zeta) + \frac{i}{2}[\overline{(1+\zeta^2)F'(\zeta)}] \\ + \frac{\Gamma}{4i}[(\zeta+i)^2 F'(\zeta) - \overline{(\zeta+i)^2 F'(\zeta)}] \\ + \overline{H(\zeta)} = iB\zeta^2, \end{aligned} \tag{41}$$

valid at the unit circle, where $F(\zeta)$ and $H(\zeta)$ are holomorphic on the elastic domain. Following the integrations of (41) and its conjugate as in the previous section, we obtain the differential equations for $F(\zeta)$ and $H(\zeta)$:

$$F(\zeta) + \frac{\Gamma}{4i}(\zeta+i)^2 F'(\zeta) = iB\zeta^2, \tag{42}$$

$$\left[-\frac{i}{2}(1+\zeta^2) + \frac{\Gamma}{4i}(\zeta+i)^2 \right] F'(\zeta) + H(\zeta) = 0. \tag{43}$$

The first-order linear differential equation for $F(\zeta)$ can be solved as

$$\begin{aligned} F(\zeta) = -\frac{4B}{\Gamma}\Bigg[\zeta + i - 2i\left(\frac{2}{\Gamma} + 1\right) \\ \times \exp\left(\frac{4i}{\Gamma(\zeta+i)}\right) \mathrm{E}_1\left(\frac{4i}{\Gamma(\zeta+i)}\right) \Bigg], \end{aligned} \tag{44}$$

with the exponential integral E_1 defined as

$$\mathrm{E}_1(\sigma) = \int_1^\infty dt \, \frac{e^{-t\sigma}}{t} \quad \text{for} \quad \mathrm{Re}(\sigma) \geqslant 0. \tag{45}$$

One verifies that indeed $\mathrm{Re}(\frac{4i}{\Gamma(\zeta+i)}) \geqslant 0$ for $|\zeta| \leqslant 1$. Substituting $\zeta + i = \frac{2}{z-i}$, we thus find the sought-for potential

$$\begin{aligned} \phi(z) = -\frac{2\mathcal{B}}{\Gamma}\Bigg[\frac{2}{z-i} - 2i\left(\frac{2}{\Gamma} + 1\right) \\ \times \exp\left(\frac{2i(z-i)}{\Gamma}\right) \mathrm{E}_1\left(\frac{2i(z-i)}{\Gamma}\right) \Bigg]. \end{aligned} \tag{46}$$

This is sufficient to compute the interface deflection $h(x) = u_y(x, y = 0) = \mathrm{Im}[\phi(x)]$; for the current case it turns out that the constant $K = 0$ to achieve vanishing displacements at infinity. However, if we wish to compute the displacements inside the elastic body, we also require the other potential $\psi(z)$. Combining (43) and (44), we obtain

$$H(\zeta) = -\frac{4Bi}{\Gamma}\left[\frac{\Gamma}{4}(\zeta+i)^2 + \frac{1}{2}(\zeta^2+1)\right]\left[1 + \frac{2i\left(\frac{2}{\Gamma}+1\right)}{\zeta+i}\left\{\frac{4i}{\Gamma(\zeta+i)}\exp\left(\frac{4i}{\Gamma(\zeta+i)}\right)\mathrm{E}_1\left(\frac{4i}{\Gamma(\zeta+i)}\right) - 1\right\}\right], \tag{47}$$

which after the substitution $\zeta + i = \frac{2}{z-i}$ yields

$$\psi(z) = -\frac{i\mathcal{B}}{2}\left(\frac{z-i}{z+i}\right)^2 - \frac{2\mathcal{B}i}{\Gamma}\frac{(\Gamma - 2iz)}{(z-i)^2}\left[1 + i\left(\frac{2}{\Gamma}+1\right)(z-i)\left\{\frac{2i(z-i)}{\Gamma}\exp\left(\frac{2i(z-i)}{\Gamma}\right)\mathrm{E}_1\left(\frac{2i(z-i)}{\Gamma}\right) - 1\right\}\right]. \tag{48}$$

2. Asymptotics

It is instructive to briefly consider the behavior for large $|(z-i)|/\Gamma$. For large arguments, the exponential integral can be expanded as

$$\exp(\sigma)\mathrm{E}_1(\sigma) = \frac{1}{\sigma} - \frac{1}{\sigma^2} + O\left(\frac{1}{\sigma^3}\right), \tag{49}$$

so that, to leading order, the potential ϕ in (46) becomes

$$\phi(z) \simeq \frac{-2\mathcal{B}}{\Gamma}\left[\frac{2}{z-i} - \frac{4i}{\Gamma}\left\{\frac{\Gamma}{2i(z-i)} - \left(\frac{\Gamma}{2i(z-i)}\right)^2\right\} - 2i\left\{\frac{\Gamma}{2i(z-i)} - \left(\frac{\Gamma}{2i(z-i)}\right)^2\right\}\right] \simeq \mathcal{B}\frac{2z + i\Gamma}{(z-i)^2}. \tag{50}$$

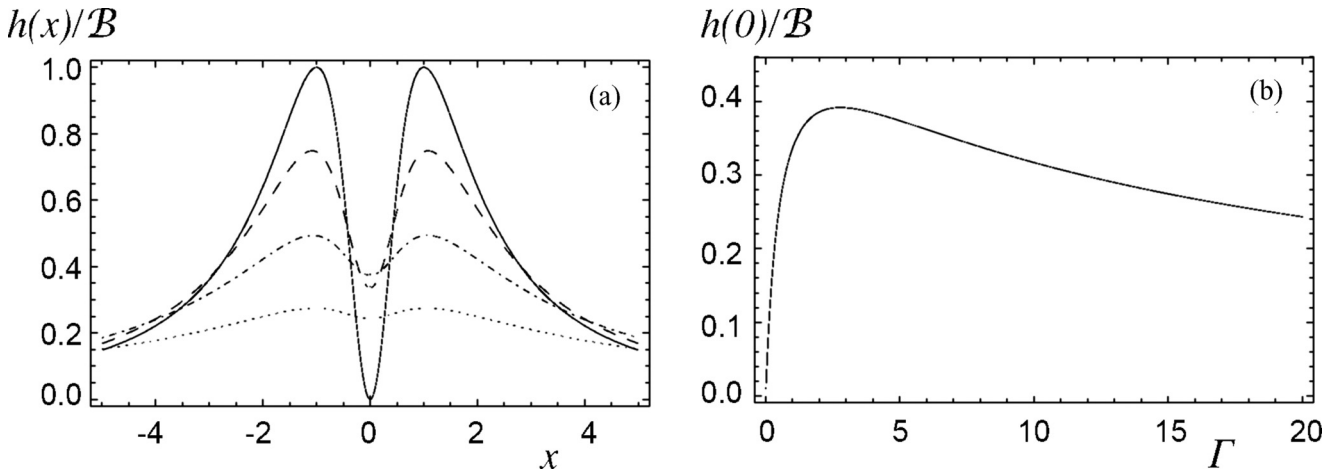

FIG. 2. (a) Interface deformation $h(x)/\mathcal{B}$ for different values of the surface tension: $\Gamma = 0$ (solid), $\Gamma = 1$ (dashed), $\Gamma = 5$ (dash-dotted), and $\Gamma = 20$ (dotted). Here, all lengths h and x are already dimensionless and scaled by d. The influence of surface tension is to smooth interface variations. (b) Central deflection $h(0)/\mathcal{B}$ exhibits a nonmonotonic dependence on surface tension Γ.

For vanishing Γ this reduces to (32), the result without surface tension (up to a redundant constant). For finite Γ, this expression provides the far-field solution valid for $|z| \gg \Gamma$. The corresponding surface deflection, for $|x| \gg \Gamma$, reads

$$h(x) \simeq (4+\Gamma)\mathcal{B}\frac{x^2}{(x^2+1)^2} = \frac{(4+\Gamma)\beta}{d^3}\frac{x^2}{(x^2+1)^2}. \quad (51)$$

The interface deformation thus decays as $1/x^2$, but with a prefactor that depends on the strength of the surface tension.

Similarly, we can perform the expansion of the exponential integral for small arguments, $\mathrm{E}_1(\sigma) \simeq -\gamma_E - \ln\sigma$, where γ_E is the Euler-Mascheroni constant. From this, one can compute for example the central height in the limit of large surface tension $\Gamma \gg 1$:

$$h(0) \simeq \frac{4\mathcal{B}\ln\Gamma}{\Gamma}, \quad (52)$$

where we kept only the dominant logarithmic factor. The interface deformations near the center will thus be suppressed at large Γ.

C. Results

Let us now discuss our findings using graphical representations. Our main goal was to compute the surface deflection of the elastic body due to the vortex dipole, and to consider the effect of surface tension. Figure 2(a) shows the corresponding profiles $h(x)$, normalized by the dipole strength $\mathcal{B} = \beta/d^3$, for different values of $\Gamma = \gamma/(\mu d)$. In all cases the interface deflection is upwards (positive) at all positions x. This is to be contrasted with the viscous case, for which the surface deflection is downwards (negative). The result for $\Gamma = 0$, given by (35), is shown as the solid line. Interestingly, this case gives no displacement at the center, $x = 0$. This could also be inferred from the streamline pattern shown in Fig. 1(c): The origin $(x = 0, y = 0)$ is a stagnation point of the displacement field. The maximum displacements are found at $x = \pm 1$.

The inclusion of surface tension leads to a reduction of the interfacial area, and hence smooths the spatial variations. However, its effect on the detailed spatial structure is rather subtle. Figure 2(a) shows that the increase of surface tension gives rise to a reduction of the maxima: The traction induced by the positive Laplace pressure locally pushes down on the elastic body. Interestingly, the displacement at $x = 0$ evolves nonmonotonically with Γ. Initially the effect of surface tension is to reduce the difference with respect to the pronounced maxima. The Laplace pressure is negative at the center, pulling up the elastic body along its center line. For very large surface tensions, however, interface deflections are suppressed over a very wide central range. This nonmononotonic behavior is summarized in Fig. 2(b), showing $h(0)/\mathcal{B}$ versus Γ. Notice the very slow decay at large Γ, which can be understood from the asymptotics (52). The width of the central region is given by $\Gamma = \gamma/(\mu d)$, or in dimensional units it is governed by the elastocapillary length γ/μ. Outside this region, the deflections decay as $1/x^2$, as described by the asymptotics (51). The amplitude of the far-field displacements is proportional to Γ: In this region the Laplace pressure is again negative, such that surface tension locally enhances the upward displacement.

Figure 3 finally represents the computed displacement fields as "streamline" patterns. As in Fig. 1, the free surface is at the top of the panels while the dipole is seen at the center line, just above the middle. The leftmost panel shows the result for $\Gamma = 0$, as was previously given in Fig. 1(c). For $\Gamma > 0$ we observe that the stagnation point of the displacement field is below the free surface: As a consequence, the displacements at the free surface are indeed in the upward direction. The topology of the fields is highlighted by the black lines, which separate streamlines that return to the dipole from those that cross the free surface. While the topology of the fields remain the same at all values of Γ, one observes a "flattening" of the contours near the center line that is due to the effect of surface tension.

IV. DISCUSSION

In summary, we have considered the elastic analog of the viscous problem considered by Jeong and Moffatt [27],

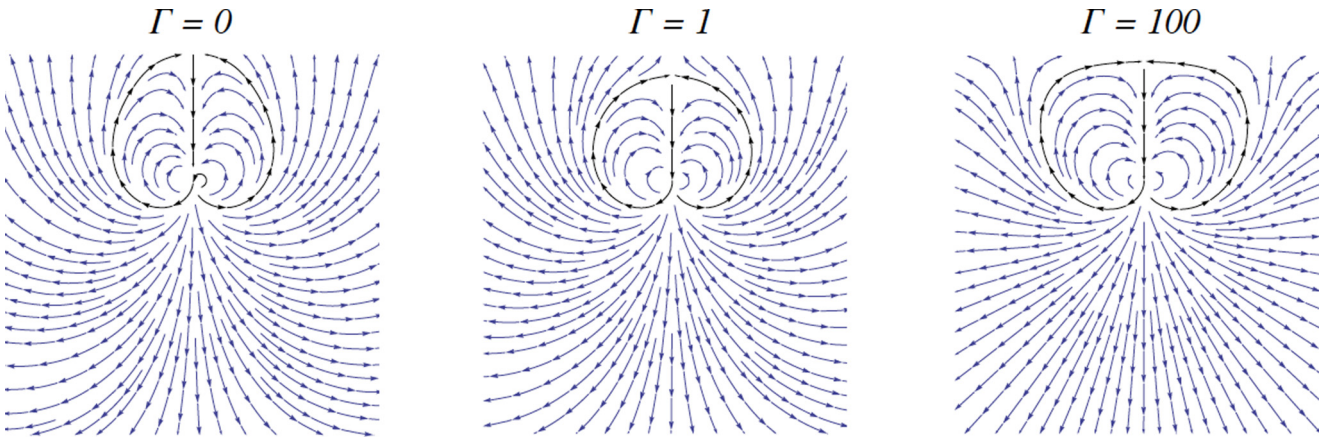

FIG. 3. (Color online) Displacement field for different surface tensions $\Gamma = \gamma/(\mu d)$, using the same scales as in Fig. 1. The position of the vortex dipole is clearly visible below the free surface. The black lines separate the streamlines that return to the dipole from those that cross the interface. Apart from the case $\Gamma = 0$, the stagnation point of the field lies below the free surface and as a consequence gives rise to an upward displacement at the free surface.

where a capillary interface is deformed due to a vortex dipole (cf. Fig. 1). Despite the equivalence of Stokes flow and the equations of linear elasticity, we found that the resulting deflections and streamline patterns are rather distinct. This can be attributed to the kinematic boundary condition of the interface, which is very different for steady viscous flow and for an elastic free surface. However, the presented elastic calculation *does* have a counterpart in the viscous flow case. Namely, the *unsteady* kinematic boundary condition reads

$$\frac{\partial h}{\partial t} = v_y|_{y=h} - v_x|_{y=h}\frac{\partial h}{\partial x}. \tag{53}$$

At steady state this reduces to the previously used (9). However, let us consider the transient flow that is achieved when the vortex dipole is started at $t = 0$ in a pool that is initially at rest. The interface is initially flat, so that the kinematic condition at early times becomes

$$\frac{\partial h}{\partial t} \simeq v_y|_{y=h}. \tag{54}$$

This is equivalent to the elastic kinematic condition (10), upon identification of $h \to \partial h/\partial t$ and $u_y \to v_y$. When counter-rotating vortices are started up in a viscous experiment, we therefore expect the flow to initially resemble the field in Fig. 1(c). The interface then initially deflects upwards, but after a short transient relaxes towards the steady flow pattern in Fig. 1(b).

The prime interest of the viscous flow problem was to study the appearance of an interfacial cusp at large driving strength [27,31–33]. Unfortunately, the limit of large deformation is beyond the realm of linear elasticity, and can thus not be assessed with the methods discussed in the present paper. However, we speculate that a free surface cusp does not form in the elastic problem. The mechanism for cusp formation in Stokes flow is that the interface is deflected towards the vortex dipole, strongly enhancing the velocities in the vicinity of the stagnation point at the center of the free surface, at $x = 0$. Our linear analysis suggests that this enhancing mechanism is not present in the elastic case, as the displacement near the free surface is *opposite* to that of the dipole. A fully nonlinear (numerical) analysis is required to resolve this question. Alternatively, an experimental approach may be attempted by embedding cylinders inside an elastic gel, which will allow a torque dipole to be exerted.

As a final remark, we note that the complex variable method could be of interest for describing other types of elastocapillary problems. A technical difficulty that is common for deformable gels is that the surface traction explicitly depends on the displacement field: Stresses and displacements thus have to be solved self-consistently. For the present case we showed that this can be resolved quite naturally within the complex variable formalism, reducing the effort to solution of a first-order differential equation.

ACKNOWLEDGMENT

J.S. acknowledges financial support from ERC (the European Research Council) Consolidator Grant No. 616918.

[1] P.-G. de Gennes, F. Brochard-Wyart, and D. Quere, *Capillarity and Wetting Phenomena: Drops, Bubbles, Pearls, Waves* (Springer, New York, 2004).
[2] S. Mora, T. Phou, J.-M. Fromental, L. M. Pismen, and Y. Pomeau, Phys. Rev. Lett. **105**, 214301 (2010).
[3] A. Marchand, S. Das, J. H. Snoeijer, and B. Andreotti, Phys. Rev. Lett. **108**, 094301 (2012).
[4] S. Mora, C. Maurini, T. Phou, J.-M. Fromental, B. Audoly, and Y. Pomeau, Phys. Rev. Lett. **111**, 114301 (2013).
[5] D. Paretkar, X. Xu, C.-Y. Hui, and A. Jagota, Soft Matter **10**, 4084 (2014).
[6] D. Long, A. Ajdari, and L. Leibler, Langmuir **12**, 5221 (1996).
[7] E. R. Jerison, Y. Xu, L. A. Wilen, and E. R. Dufresne, Phys. Rev. Lett. **106**, 186103 (2011).

[8] A. Marchand, S. Das, J. H. Snoeijer, and B. Andreotti, Phys. Rev. Lett. **109**, 236101 (2012).
[9] L. Limat, Eur. Phys. J. E **35**, 134 (2012).
[10] R. W. Style and E. R. Dufresne, Soft Matter **8**, 7177 (2012).
[11] L. A. Lubbers, J. H. Weijs, L. Botto, S. Das, B. Andreotti, and J. H. Snoeijer, J. Fluid. Mech. **747**, R1 (2014).
[12] J. Bostwick, M. Shearer, and K. Daniels, Soft Matter **10**, 7361 (2014).
[13] R. W. Style, C. Hyland, R. Boltyanskiy, J. S. Wettlaufer, and E. R. Dufresne, Nat. Commun. **4**, 2728 (2013).
[14] T. Salez, M. Benzaquen, and E. Raphael, Soft Matter **9**, 10699 (2013).
[15] J. Harden, H. Pleiner, and P. Pincus, J. Chem. Phys. **94**, 5208 (1991).
[16] F. Monroy and D. Langevin, Phys. Rev. Lett. **81**, 3167 (1998).
[17] R. Pericet-Camara, E. Bonaccurso, and K. Graf, ChemPhysChem **9**, 1738 (2008).
[18] R. W. Style, R. Boltyanskiy, Y. Che, J. S. Wettlaufer, L. A. Wilen, and E. R. Dufresne, Phys. Rev. Lett. **110**, 066103 (2013).
[19] T. Kajiya, A. Daerr, T. Narita, L. Royon, F. Lequeux, and L. Limat, Soft Matter **9**, 454 (2013).
[20] J. H. Michell, Proc. London Math. Soc. **100**, 100 (1899).
[21] W. R. Dean and P. E. Montagnon, Proc. Cambridge Philos. Soc. **45**, 389 (1949).
[22] H. K. Moffatt, J. Fluid Mech. **18**, 1 (1964).
[23] C. Huh and L. E. Scriven, J. Coll.oid Interface Sci. **35**, 85 (1971).
[24] H. K. Moffatt and B. R. Duffy, J. Fluid Mech. **96**, 299 (1980).
[25] D. Anderson and S. Davis, J. Fluid Mech. **257**, 1 (1993).
[26] H. Gelderblom, O. Bloemen, and J. H. Snoeijer, J. Fluid Mech. **709**, 69 (2012).
[27] J.-T. Jeong and H. K. Moffatt, J. Fluid Mech. **241**, 1 (1992).
[28] R. Hopper, J. Fluid Mech. **213**, 349 (1990).
[29] J. Eggers, J. R. Lister, and H. A. Stone, J. Fluid Mech. **401**, 293 (1999).
[30] N. Muskhelishvili, *Some Basic Problems of the Mathematical Theory of Elasticity* (Noordhoff, Leiden, Netherlands, 1977).
[31] D. D. Joseph, J. Nelson, M. Renardy, and Y. Renardy, J. Fluid Mech. **223**, 383 (1991).
[32] J. Eggers, Phys. Rev. Lett. **86**, 4290 (2001).
[33] E. Lorenceau, F. Restagno, and D. Quéré, Phys. Rev. Lett. **90**, 184501 (2003).
[34] R. Shuttleworth, Proc. Phys. Soc., London, Sect. A **63**, 444 (1950).
[35] P. Muller and A. Saul, Surf. Sci. Rep. **54**, 157 (2004).
[36] J. H. Weijs, B. Andreotti, and J. Snoeijer, Soft Matter **9**, 8494 (2013).